Ultrasonics Sonochemistry 26 (2015) 30–39

Contents lists available at ScienceDirect

Ultrasonics Sonochemistry

journal homepage: www.elsevier.com/locate/ultson

Comprehensive experimental and numerical investigations of the effect of frequency and acoustic intensity on the sonolytic degradation of naphthol blue black in water

Hamza Ferkous [a], Slimane Merouani [a,b,*], Oualid Hamdaoui [a], Yacine Rezgui [c], Miloud Guemini [c]

[a] Laboratory of Environmental Engineering, Department of Process Engineering, Faculty of Engineering, Badji Mokhtar – Annaba University, P.O. Box 12, 23000 Annaba, Algeria
[b] Department of Chemical Engineering, Faculty of Pharmaceutical Engineering Process, University of Constantine 3, Constantine, Algeria
[c] Laboratory of Applied Chemistry and Materials Technology, University of Oum El-Bouaghi, P.O. Box 358, 04000 Oum El Bouaghi, Algeria

ARTICLE INFO

Article history:
Received 5 December 2014
Received in revised form 1 February 2015
Accepted 2 February 2015
Available online 7 February 2015

Keywords:
Sonochemical degradation
Naphthol blue black (NBB)
Numerical simulations
Frequency
Acoustic intensity
·OH radical

ABSTRACT

In the present work, comprehensive experimental and numerical investigations of the effects of frequency and acoustic intensity on the sonochemical degradation of naphthol blue black (NBB) in water have been carried out. The experiments have been examined at three frequencies (585, 860 and 1140 kHz) and over a wide range of acoustic intensities. The observed experimental results have been discussed using a more realistic approach that combines the single bubble sonochemistry and the number of active bubbles. The single bubble yield has been predicted using a model that combines the bubble dynamics with chemical kinetics consisting of series of chemical reactions (73 reversible reactions) occurring inside an air bubble during the strong collapse. The experimental results showed that the sonochemical degradation rate of NBB increased substantially with increasing acoustic intensity and decreased with increasing ultrasound frequency. The numerical simulations revealed that NBB degraded mainly through the reaction with hydroxyl radical (·OH), which is the dominant oxidant detected in the bubble during collapse. The production rate of ·OH radical inside a single bubble followed the same trend as that of NBB degradation rate. It increased with increasing acoustic intensity and decreased with increasing frequency. The enhancing effect of acoustic intensity toward the degradation of NBB was attributed to the rise of both the individual chemical bubble yield and the number of active bubbles with increasing acoustic intensity. The reducing effect of frequency was attributed to the sharp decrease in the chemical bubble yield with increasing frequency, which would not compensated by the rise of the number of active bubbles with the increase in ultrasound frequency.

1. Introduction

Water pollution due to discharge of colored effluents from textile dye manufacturing is one of the major environmental concerns in today's world. Strong color imparted by dyes to the receiving aquatic ecosystems poses aesthetic problems as well as serious ecological problems, such as carcinogenicity and inhibition of benthic photosynthesis [1]. Azo dyes have been widely used as colorants in a variety of products such as textiles, paper and leather. Approximately half of all known dyes are azo dyes, making them the largest group of synthetic colorants [2]. These chemicals present a potential human health risk as some of them have been shown to be carcinogenic [3]. Traditional methods for dye removal include biological treatment [4,5], coagulation [6,7], filtration [8] and adsorption [9–11]; however, because of high dye concentrations and the increased stability of synthetic dyes, these methods are becoming less effective for the treatment of colored industry effluents. To overcome the problems associated with these traditional methods, much attention has recently been focused on the so-called advanced oxidation processes for water and wastewater decontamination. In these processes various techniques (e.g. photocatalysis, Fenton reaction, UV/H_2O_2) are applied to produce reactive species [12–14], principally, hydroxyl radicals (·OH), which are able to induce the degradation and mineralization of organic pollutants [15].

A new way of generating of ·OH radials is the application of ultrasound in the frequency range 20–1000 kHz, in which case important sonochemical effects can be observed [16,17]. Application of ultrasound to aqueous solutions induces the

* Corresponding author at: Department of Chemical Engineering, Faculty of Pharmaceutical Engineering Process, University of Constantine 3, Constantine, Algeria. Tel./fax: +213 38876560.
E-mail addresses: s.merouani@yahoo.fr, s.merouani03@gmail.com (S. Merouani).

http://dx.doi.org/10.1016/j.ultsonch.2015.02.004
1350-4177/

Nomenclature

c	speed of sound in the liquid medium (m s^{-1})
f	frequency of ultrasonic wave (Hz)
I_a	acoustic intensity of ultrasonic irradiation (W m^{-2})
I	number of chemical reactions
$k_{NBB\text{-}OH}$	Liquid rate constant of NBB with ·OH
p	pressure inside a bubble (Pa)
P_A	amplitude of the acoustic pressure (Pa)
P_{g0}	initial gas pressure (Pa)
P_v	vapor pressure of water (Pa)
$p_s(t)$	acoustic pressure
p_∞	ambient static pressure (Pa)
R	radius of the bubble (m)
R_{max}	maximum radius of the bubble (m)
R_{min}	minimum radius of the bubble at the collapse (m)
R_0	ambient bubble radius (m)
t	time (s)
T	temperature inside a bubble (K)
T_∞	ambient liquid temperature (K)
X	symbol of chemical species

Greek letters

γ	specific heat ratio (c_p/c_v) of the gas mixture
σ	surface tension of liquid water (N m^{-1})
ρ	density of liquid water (kg m^{-3})
μ	viscosity of liquid water (N m^{-2} s)

formation of vapor and gas-filled microbubbles that grow and then adiabatically collapse causing temperatures of about 5000 K and pressures in excess of 500 atm within the bubbles [18,19]. These extremely conditions inducing the pyrolysis of water vapor, oxygen molecules and volatile organic compounds that can be present in the gas phase [18]. Pyrolysis of water vapor yields hydroxyl radicals (·OH) and hydrogen atoms (H·) [19]. These active species can recombine, react with other gaseous species present in the cavity to form other active species such as HO_2· and O, or diffuse out of the bubble into the bulk liquid medium [20]. Hydroxyl radicals in particular are very reactive and can transform dissolved organic compounds [21]. Reactions can take place in the gas phase, at the gas–liquid interface and in the solution bulk after transfer of gaseous radicals into the liquid phase [20]. Accordingly, the sonochemical degradation of an organic compound can be influenced by its physicochemical properties. An organic pollutant with high volatility character will be incinerated in the bubble whereas a hydrophilic or hydrophobic compound with low volatility cannot enter the bubble, but will be oxidized in the bulk solution or interfacial area by reaction with ·OH radicals [16,18].

The most crucial parameters for application of sonolysis are the employed frequency and power. Although the effect of these two parameters on the sonochemical degradation of organic pollutants has been widely examined [22–27], comprehensive studies on the effects of frequency and power are yet to be carried out. The present study provides a comprehensive experimental and numerical investigation of the effects of frequency and acoustic intensity on the sonochemical degradation of organic matters. Naphthol blue black (NBB), an acidic dye of the diazo class, was chosen as substrate model. NBB is widely used in the textile industry for dyeing wool, nylon, silk and textile printing [28]. It is characterized by a high photo- and thermal stability [28]. The experiments have been examined at three frequencies (585, 860 and 1140 kHz) and over a wide range of acoustic intensities. The observed experimental results have been discussed with respect to single bubble sonochemistry and the number of active bubbles. The chemical bubble yield has been predicted using a model that combines the bubble dynamics with chemical kinetics consisting of series of chemical reactions (73 reversible reactions) occurring inside a reactive cavitating bubble.

2. Materials and methods

2.1. Reagents

Naphthol blue black (abbreviation: NBB; Acid Black 1; C.I. number: 1064-48-8; chemical class: azo dye; molecular formula: $C_{22}H_{14}N_6Na_2O_9S_2$, molecular weight: 616.49 g mol^{-1}) was supplied by Sigma–Aldrich and used without any purification. The molecular structure of NBB was shown in Fig. 1.

2.2. Ultrasonic reactor

Sonolysis experiments were conducted in a cylindrical water-jacketed glass reactor (Fig. 2). The ultrasonic waves at 585, 860 and 1140 kHz were delivered from the bottom through a Meinhardt multifrequency transducer (model E/805/T/M, diameter of the active area 5.3 cm). The generator that aliments the multifrequency transducer operates at various electrical powers that are indicated by a fixed three positions, namely, amp 2, amp 3 and amp 4. The temperature of the solution was monitored using a thermocouple immersed in the reacting medium. Acoustic power dissipated in the reactor was estimated under different conditions using a standard calorimetric method [29,30].

2.3. Procedures

All NBB solutions were prepared with distilled water. Sonochemical experiments were carried out under different conditions using constant solution volume of 300 mL. Aqueous samples were taken periodically from the solution and the concentrations of the dye were determined using a UV–visible spectrophotometer (Lightwave II) at 620 nm. The temperature of the sonicated solution was kept at 25 °C by circulating cooling water through a jacket surrounding the cell. In all the cases, the reactor was open to air and the experiments were carried out at natural pH (pH ~ 6).

3. Theoretical package

The theoretical model used for studying the single bubble sonochemistry at different conditions of frequency and acoustic intensity has been fully described in our previous papers [31,32]. The model combines the dynamic of single bubble with chemical kinetics occurring inside a bubble during the collapse. The following is a brief description of the model.

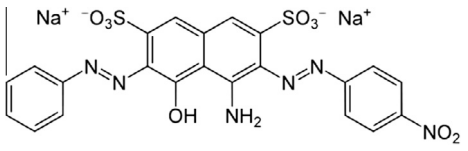

Fig. 1. Molecular structure of NBB.

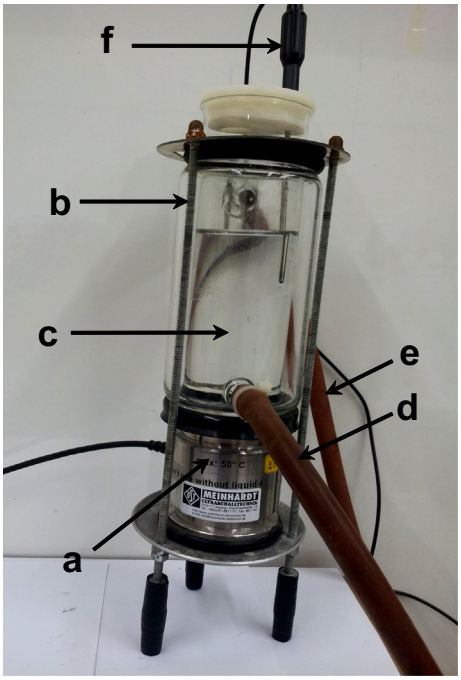

Fig. 2. Sonochemical reactor used for the degradation of NBB. (a) Meinhardt multi-frequency transducer operating at 585, 860 and 1140 kHz, (b) cylindrical jacketed glass cell, (c) sonicated solution, (d) inlet cooling water, (e) outlet cooling water and (f) thermocouple.

3.1. Bubble dynamics model

A gas and vapor filled spherical bubble isolated in water oscillates under the action of a sinusoidal sound wave. The temperature and pressure in the bubble are assumed spatially uniform and the gas content of the bubble behaves as an ideal gas [33]. The radial dynamics of the bubble is described by the Keller–Miksis equation that includes first order terms in the Mach number $M = \dot{R}/c$ [34,35]:

$$\left(1-\frac{\dot{R}}{c}\right)R\ddot{R}+\frac{3}{2}\left(1-\frac{\dot{R}}{3c}\right)\dot{R}^2=\frac{1}{\rho_L}\left(1+\frac{\dot{R}}{c}+\frac{R}{c}\frac{d}{dt}\right)\times\left[p-p_\infty-\frac{2\sigma}{R}-4\mu\frac{\dot{R}}{R}-p_s(t)\right] \quad (1)$$

in this equation dots denote time derivatives (d/dt), R is the radius of the bubble, c is the speed of sound in the liquid, ρ_L is the density of the liquid, σ is the surface tension, μ is the liquid viscosity, p is the pressure inside the bubble, p_∞ is the ambient static pressure and $p_s(t)$ is the time-dependent pressure field driving the bubble into oscillation. In the case of bath-type sonochemical reactor, actual acoustic field in the reactor is a damped standing-wave field [36]. However, when a bubble is irradiated by an acoustic wave whose wavelength is much longer than the bubble radius, the acoustic pressure can be described assuming a traveling-wave field as follows [37,38]: $p_s(t) = -P_A \sin(2\pi ft)$, where P_A is the acoustic amplitude of the acoustic wave and f is its frequency. The acoustic amplitude P_A is correlated with the acoustic intensity I_a, or power per unit area, as $P_A = (2I_a\rho_L c)^{1/2}$ [16].

The expansion of the bubble is assumed as isothermal and its total compression is considered as adiabatic [39,40]. These assumptions, which are widely accepted since the lifetime of an oscillation at high frequency is relatively short with a very rapidly occurring collapse event, were pointed out by Yasui et al. [41] using a more detailed model. We also assume that the vapor pressure in the bubble remains constant during the bubble expansion phase and there is no gas diffusion during expansion and no mass and heat transfer of any kind during collapse. Storey and Szeri [42] demonstrated that the inclusion of mass transfer on the bubble dynamics has practically no effect on the maximum bubble temperature attained in the bubble at the collapse when the compression ratio of the bubble (R_{max}/R_{min}) is less than 20 (R_{max} is the maximum radius of the bubble and R_{min} is the minimum bubble radius at the collapse). This level of R_{max}/R_{min} was never attained in the present numerical study. Therefore, in order to reduce computational parameters, the current model takes, as input, initial bubble vapor content and neglects mass and heat transfer during bubble expansion and collapse.

Because of the above assumptions, the pressure and temperature inside the bubble at any instant during adiabatic phase can be calculated from the bubble size as

$$p=\left[P_v+P_{g0}\left(\frac{R_0}{R_{max}}\right)^3\right]\left(\frac{R_{max}}{R}\right)^{3\gamma} \quad (2)$$

$$T=T_\infty\left(\frac{R_{max}}{R}\right)^{3(\gamma-1)} \quad (3)$$

where P_v is the vapor pressure, $P_{g0} = p_\infty + (2\sigma/R_0) - P_v$ is the gas pressure in the bubble at its ambient state ($R = R_0$), R_0 is the ambient bubble radius, T_∞ is the bulk liquid temperature and γ is the ratio of specific heats capacities (c_p/c_v) of the gas/vapor mixture, given as

$$\gamma=\sum_{k=1}^{K}y_k\gamma_k \quad (4)$$

when y_k is the mole fraction of the species k at time corresponding to $R = R_{max}$ and γ_k is the ratio of specific heat capacities of the species k, which will be assumed constant.

It is important to notice also that the assumption of spatial uniform pressure and temperature inside the bubble is valid as long as inertia effects are negligible and the velocity of the bubble wall is below the speed of sound in the vapor/gas mixture. This assumption was justified in detail in the paper published by Kamath et al. [43]. In addition, Yasui et al. [41] and Fujikawa and Akamatzu [44] pointed out in their complete models which include heat transfer that the bubble temperature and pressure are roughly uniform except at a very thin layer, called thermal boundary, near the bubble wall.

3.2. Chemical kinetics model

For simulating the chemical reactions occurring inside the bubble, a kinetic mechanism consisting in 73 chemical reactions and their backwards reactions (Table 2 in Ref. [45]) is taken into account including O_2, H_2O, $^{\cdot}OH$, $H^{\cdot}$, O, $HO_2^{\cdot}$, O_3, H_2, H_2O_2, N_2, N, NO, NO_2, NO_3, HNO_2, HNO_3, N_2O, HNO, NH, NH_2, NH_3, N_2H_2, N_2H_3, N_2H_4, N_2O_4 and N_2O_5 species. The used scheme has been partially validated from hydrogen flame studies [46] as well as shock-tube and reactor-type experiments [47]. It has also been validated from studies of single bubble sonochemistry [37].

The adopted chemical kinetics model consists of the reaction mechanism and determines the production of each species during the bubble collapse. Rate expressions for the chemical reactions consider elementary reversible reactions involving K chemical species, which can be represented in the general form as

$$\sum_{k=1}^{K}\upsilon'_{ki}X_k \leftrightarrow \sum_{k=1}^{K}\upsilon''_{ki}X_k \quad (5)$$

in which υ_{ki} in the stoichiometric coefficients of the ith reaction and X_k is the chemical symbol for the kth species. The superscript $'$ indicates forward stoichiometric coefficients, while $''$ indicates reverse

stoichiometric coefficients. The production rate $w_{\bullet k}$ of the kth species can be written as a summation of the rate of the variables for all reactions involving the kth species:

$$\dot{w}_k = \sum_{i=1}^{I} (\upsilon''_{ki} - \upsilon'_{ki}) r_i \quad (k = 1, \ldots, K) \tag{6}$$

The rate r_i for the ith reaction is given by the difference of the forward and reverse rates as

$$r_i = k_{f_i} \prod_{k=1}^{K} [X_k]^{\upsilon'_{ki}} - k_{ri} \prod_{k=1}^{K} [X_k]^{\upsilon''_{ki}} \tag{7}$$

where $[X_k]$ is the molar concentration of the kth species and k_{fi} and k_{ri} are the forward and reverse rate constants of the ith reaction, respectively. The forward and reverse rate constants for the ith reactions are assumed to have the following Arrhenius temperature dependence:

$$k_{f_i} = A_{f_i} T^{b_{f_i}} \exp\left(-\frac{E_{af_i}}{R_g T}\right) \tag{8}$$

$$k_{ri} = A_{ri} T^{b_{ri}} \exp\left(-\frac{E_{a_{ri}}}{R_g T}\right) \tag{9}$$

where R_g is the universal gas constant, A_{fi} (A_{ri}) is the pre-exponential factor, b_{fi} (b_{ri}) is the temperature exponent and E_{fi} (E_{ri}) is the activation energy. Arrhenius parameters of the important reactions inside an air bubble, listed in Table 1, were obtained from the NIST Chemical Kinetics Database [48] and other bibliographic references [39,43,46,47].

3.3. Procedure of the numerical simulation

The numerical procedure used for solving the bubble dynamic equation and simulating the reactions systems inside a bubble have been presented in detail in our previous work [31]. Briefly, the Keller–Miksis equation (Eq. (1)), describing the dynamic of the bubble, is a non-linear second-order differential equation which requires an approximate numerical method for solution. It has been solved by the fourth-order Runge–Kutta method using the initial conditions: $t = 0$, $R = R_0$ and $dR/dt = 0$. The simulation of the chemical reactions in the bubble (73 chemical reactions) starts at the beginning of the adiabatic phase (at time corresponding to $R = R_{max}$). The application of Eq. (6) for all species involved in the used chemical kinetics mechanism (26 species) gives a system of 26 ordinary differential equations. The input parameters for solving the system of the ordinary differential equations are the composition of the bubble on water vapor and air at the time corresponding to $R = R_{max}$, the temperature and pressure profiles in the bubble during adiabatic phase and the collapse time. These parameters are obtained by solving the dynamic equation (Eq. (1)). As the bubble temperature increases during the adiabatic phase, the reaction system evolves and radicals start to form by thermal dissociation of H_2O and other molecules in the bubble. Thus, the composition of the bubble on all species expected to be present was determined at any temperature during the collapse period by solving the system of the ordinary differential equations obtained by Eq. (6). The system of the ordinary differential equations was solved by the finite difference method. The computer simulation of the reactions system was stopped after the end of the bubble collapse.

4. Results and discussion

4.1. Experimental section

In order to calibrate the ultrasonic reactor, experiments were carried out using water to determine the acoustic powers dissipated in the solution at different operating conditions of frequency

Table 1
The important chemical reactions inside a collapsing air/water vapor bubble when the maximum bubble temperature is 4190 K, which is the maximum temperature of the bubble at 585 kHz and 3.58 W cm^{-2}. This series of reactions are selected by analyzing the results of the chemical kinetics. M is the third body. Subscript "f" denotes the forward reaction and "r" denotes the reverse reaction. A is in (cm^3 mol^{-1} s^{-1}) for two body reaction [(cm^6 mol^{-2} s^{-1}) for a three body reaction], and E_a is in (cal mol^{-1}).

N°	Chemical reaction	A_f	b_f	E_{af}	A_r	b_r	E_{ar}
1	$H_2O + M \rightleftharpoons H^{\cdot} + {}^{\cdot}OH + M$	1.912×10^{23}	−1.83	1.185×10^{5}	2.2×10^{22}	−2.0	0.0
2	$O_2 + M \rightleftharpoons O + O + M$	4.515×10^{17}	−0.64	1.189×10^{5}	6.165×10^{15}	−0.5	0.0
3	$H^{\cdot} + O_2 \rightleftharpoons O + {}^{\cdot}OH$	1.915×10^{14}	0.0	1.644×10^{4}	5.481×10^{11}	0.39	-2.93×10^{2}
4	${}^{\cdot}OH + M \rightleftharpoons O + H^{\cdot} + M$	9.88×10^{17}	−0.74	1.021×10^{5}	4.714×10^{18}	−1.0	0.0
5	$H^{\cdot} + O_2 + M \rightleftharpoons HO_2^{\cdot} + M$	1.475×10^{12}	0.6	0.0	3.09×10^{12}	0.53	4.887×10^{4}
6	$O + H_2O \rightleftharpoons {}^{\cdot}OH + {}^{\cdot}OH$	2.97×10^{6}	2.02	1.34×10^{4}	1.465×10^{5}	2.11	-2.904×10^{3}
7	$HO_2^{\cdot} + O \rightleftharpoons {}^{\cdot}OH + O_2$	3.25×10^{13}	0.0	0.0	3.252×10^{12}	0.33	5.328×10^{4}
8	$HO_2^{\cdot} + H^{\cdot} \rightleftharpoons {}^{\cdot}OH + {}^{\cdot}OH$	7.079×10^{13}	0.0	2.95×10^{2}	2.027×10^{10}	0.72	3.684×10^{4}
9	$O + H_2 \rightleftharpoons H^{\cdot} + {}^{\cdot}OH$	3.82×10^{12}	0.0	7.948×10^{3}	2.667×10^{4}	2.65	4.88×10^{3}
10	$H^{\cdot} + H_2O \rightleftharpoons {}^{\cdot}OH + H_2$	2.298×10^{9}	1.40	1.832×10^{4}	2.16×10^{8}	1.52	3.45×10^{3}
11	$H_2O + HO_2^{\cdot} \rightleftharpoons H_2O_2 + {}^{\cdot}OH$	1.838×10^{10}	0.59	3.089×10^{4}	1.0×10^{12}	0.0	0.0
12	$H_2 + HO_2^{\cdot} \rightleftharpoons H_2O_2 + H^{\cdot}$	1.041×10^{11}	0.70	2.395×10^{4}	6.025×10^{13}	0.0	7.95×10^{3}
13	${}^{\cdot}OH + HO_2^{\cdot} \rightleftharpoons H_2O_2 + O$	8.66×10^{3}	2.68	1.856×10^{4}	9.550×10^{6}	2.0	3.97×10^{3}
14	${}^{\cdot}OH + {}^{\cdot}OH + M \rightleftharpoons H_2O_2 + M$	2.951×10^{14}	0.0	4.843×10^{4}	1.0×10^{14}	−0.37	0.0
15	$O_2 + O + M \rightleftharpoons O_3 + M$	4.1×10^{12}	0.0	-2.114×10^{3}	2.48×10^{14}	0.0	2.286×10^{4}
16	$OH + O_2 \rightleftharpoons O_3 + H$	4.4×10^{7}	1.44	7.72×10^{4}	2.3×10^{11}	0.75	0.0
17	$O + N_2 \rightleftharpoons NO + N$	7.60×10^{13}	0.0	7.60×10^{4}	1.60×10^{13}	0.0	0.00
18	$NO + HO_2^{\cdot} \rightleftharpoons OH + NO_2$	3.0×10^{12}	0.5	2.4×10^{3}	1.0×10^{11}	0.5	1.2×10^{4}
19	$NO_2 + M \rightleftharpoons O + NO + M$	1.1×10^{16}	0.0	6.6×10^{4}	1.1×10^{15}	0.0	-1.88×10^{3}
20	$NO_2 + NO_2 \rightleftharpoons NO + NO_3$	3.90×10^{11}	0.0	2.400×10^{4}	4.1×10^{14}	0.0	9.62×10^{2}
21	$NO_2 + O + M \rightleftharpoons NO_3 + M$	1.1×10^{19}	0.0	0.0	2.5×10^{9}	0.0	0.0
22	$NO_3 + H \rightleftharpoons OH + NO_2$	3.5×10^{14}	0.0	1.5×10^{3}	–	–	–
23	$N_2 + O + M \rightleftharpoons N_2O + M$	1.40×10^{12}	0.0	2.08×10^{4}	5.0×10^{14}	0.0	5.8×10^{4}
24	$OH + NO + M \rightleftharpoons HNO_2 + M$	8.0×10^{15}	0.0	-1.0×10^{3}	5.10×10^{17}	−1.0	5.000×10^{4}
25	$HNO_2 + H \rightleftharpoons H_2 + NO_2$	4.9×10^{11}	0.5	3.00×10^{3}	2.40×10^{13}	0.0	2.90×10^{4}
26	$H_2O + NO_2 \rightleftharpoons OH + HNO_2$	8.40×10^{11}	0.0	4.227×10^{4}	1.5×10^{12}	0.0	5.60×10^{1}
27	$O + HNO_2 \rightleftharpoons HNO + O_2$	3.0×10^{12}	0.0	1.60×10^{4}	–	–	–
28	$HNO + M \rightleftharpoons H + NO + M$	3.0×10^{16}	0.0	4.9×10^{4}	5.4×10^{15}	0.0	-3.0×10^{2}
29	$HNO + O \rightleftharpoons OH + NO$	4.9×10^{11}	0.5	2.0×10^{3}	–	–	–
30	$OH + NO_2 + M \rightleftharpoons HNO_3 + M$	5.0×10^{17}	0.0	0.0	1.6×10^{15}	0.0	3.08×10^{4}

and power (electrical position) using the standard calorimetric method [29,30]. The obtained results are presented in Table 2 in term of acoustic power and intensity as function of electrical position. Based on the results of the degradation experiments, the obtained ranges of acoustic power are in an interval between the cavitation threshold and a maximum intensity above which the sonochemical effects are attenuated [49].

The change in the UV–vis. spectra of the dye solution during the sonication of 30 mg L^{-1} of NBB at 585 kHz and 3.58 W cm^{-2} is shown in Fig. 3. Before sonolysis, the absorption spectrum presents two main bands: the first is in the visible region (color), with a maximum absorption at 620 nm, and the second is in the UV region, with a maximum absorption at 322 nm, which related to the absorbance of polyaromatic rings [50]. It was observed that the absorbance at 322 nm and 620 nm decreased during the initial 50 min of sonication (the decay of the 322 nm absorbance was 35%) while a new absorption peak appeared at 206 nm, indicating the degradation of the dye and the formation of intermediates, by-products and nitrate and nitrite that absorb strongly in this region. Under the same conditions, total color decay was 79%. When the reaction progressed (50> min), the absorption peaks at 622 nm and 322 nm completely disappeared and the intensity of the 206 nm peak increased with increasing irradiation time, indicating the increase in the concentration of the NBB by-products.

In Fig. 4(a)–(c), the experimental results (in term of kinetics of degradation) obtained during the ultrasonic treatment of 30 mg L^{-1} of NBB at different frequencies (585, 860 and 1140 kHz) and over a wide range of acoustic intensity (0.44–5.22 W cm^{-2}) are reported. These figures clearly show that ultrasound is effective for degrading NBB and that the operating frequency and acoustic intensity influence the efficiency of sonication. For each curve, the NBB concentration decreased exponentially with time. As mentioned early, the two major pathways for the sonochemical degradation of organic compounds in aqueous solution are: (i) thermal decomposition of volatile pollutant molecules entrapped inside the bubble and (ii) the reaction of ·OH radicals with the nonvolatile solute at the bubble interface and in the bulk solution [16,18]. NBB cannot be degraded by pyrolysis inside the cavitation bubble since its Henry's law constant is very low (1.2×10^{-31} atm m^3 mol^{-1} [51]), which suggests very low fugacity. Moreover, due to its high solubility in water (>100 g L^{-1} [51]) and low vapor pressure (4.8×10^{-29} mm Hg at 25 °C [51]), NBB may be degraded only through reaction with hydroxyl radicals (·OH) at the bubble–liquid interface and in the bulk solution:

$$\mathrm{NBB} + {\cdot}\mathrm{OH} \rightarrow\rightarrow \text{Products} \quad (10)$$

Thus, the rate of NBB oxidation is limited by the quantity of hydroxyl radicals diffused from the bubbles to the liquid ($-d[\mathrm{NBB}]/dt = k_{NBB\text{-}OH}$ [NBB] [·OH], where $k_{NBB\text{-}OH}$ is the rate constant).

From Fig. 4(a)–(c), it was obviously seen that the higher the acoustic intensity, the higher will be the removal efficiency. For example, after 80 min of sonication at 585 kHz, the NBB elimination achieved 32% at 0.44 W cm^{-2}, but the removal efficiency increased to 73 and 100% when the acoustic intensity was increased to 1.72 and 3.58 W cm^{-2}, respectively. The same trend was observed for the other frequencies. However, as the acoustic

Table 2
Estimated acoustic power and intensity dissipated in the solution (300 mL) at different conditions of frequency and electrical position. Results obtained using the calorimetric method.

Frequency	585 kHz		680 kHz		1140 kHz	
Electrical Position	Acoustic power (W)	Intensity (W cm^{-2})	Acoustic power (W)	Intensity (W cm^{-2})	Acoustic power (W)	Intensity (W cm^{-2})
Amp 2	9.65	0.44	12.33	0.56	15	0.68
Amp 3	38	1.72	51	2.31	48	2.18
Amp 4	79	3.58	107.34	4.87	115	5.22

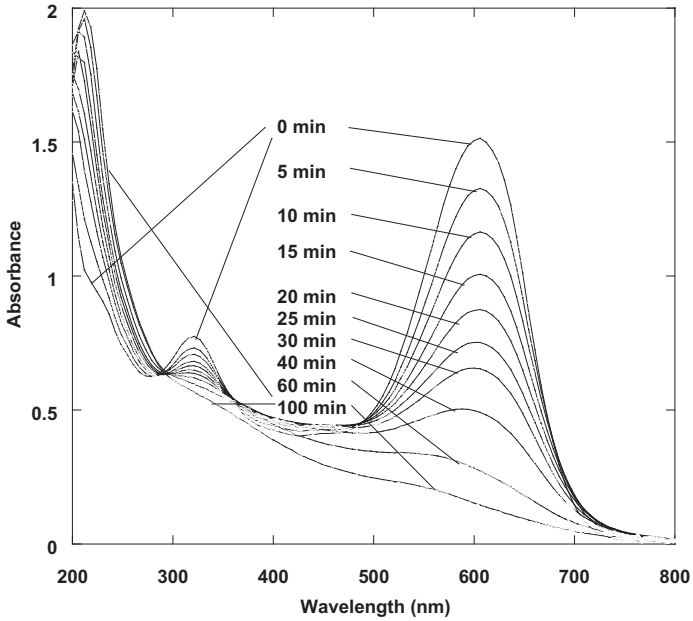

Fig. 3. Time evolution of the UV–vis. spectra of NBB solution upon ultrasonic action (conditions: volume: 300 mL, initial NBB concentration: 30 mg L^{-1}, temperature: 25 °C, natural pH, frequency: 585 kHz, acoustic intensity: 3.58 W cm^{-2}).

intensities are not the same for all frequencies, as shown in Table 2, the initial degradation rate was used to show the effect of ultrasound frequency. At this point, it should be mentioned that previous efforts have demonstrated that the degradation rate of NBB cannot be associated with a first-order law [52] and, thus, the comparisons using the initial degradation rate rather than the pseudo-first order kinetic constant is well justified. In Fig. 5, the initial degradation rate of NBB is shown as function of acoustic intensity at 585, 860 and 1140 kHz. It was seen that the initial degradation rate increased substantially with increasing acoustic intensity and decreased with increasing frequency. At 585 and 1140 kHz, the curves are nearly linear. For the lower acoustic intensities, it was also observed that the difference between the degradation rate at 585 and 860 kHz was not very notable.

4.2. Numerical section

In order to understand the results presented in Fig. 5 in term of frequency and acoustic intensity effects on the sonochemical degradation rate of NBB, it is necessary to consider the factors that influence the overall sonochemical degradation of the pollutant. As noted previously, sonochemical reaction depend upper on the single bubble event and the number of active bubbles. The active bubbles are those bubbles that collapse violently and are capable for producing chemical oxidant, i.e. ·OH radicals. In this work, a developed model for single bubble sonochemistry (described in Section 3) have been used to estimate the production rate of ·OH radical inside a single oscillating active bubble under different experimental conditions of frequency and acoustic intensity whereas the number of active bubbles where discussed qualitatively according to literature reports.

4.2.1. Single-bubble yield dependence of frequency and acoustic intensity

Numerical simulations of bubble oscillation and chemical reactions inside an isolated spherical air/water vapor bubble have been performed at various ultrasonic frequencies (585, 860 and 1140 kHz) and different acoustic intensities (Table 2). According to the experimental data reported in Refs. [53,54], the ambient radius (R_0) of a typical active bubble is strongly frequency dependent. The range of ambient bubble radius for a typical active bubble is rather narrow according to the experimental observations and it

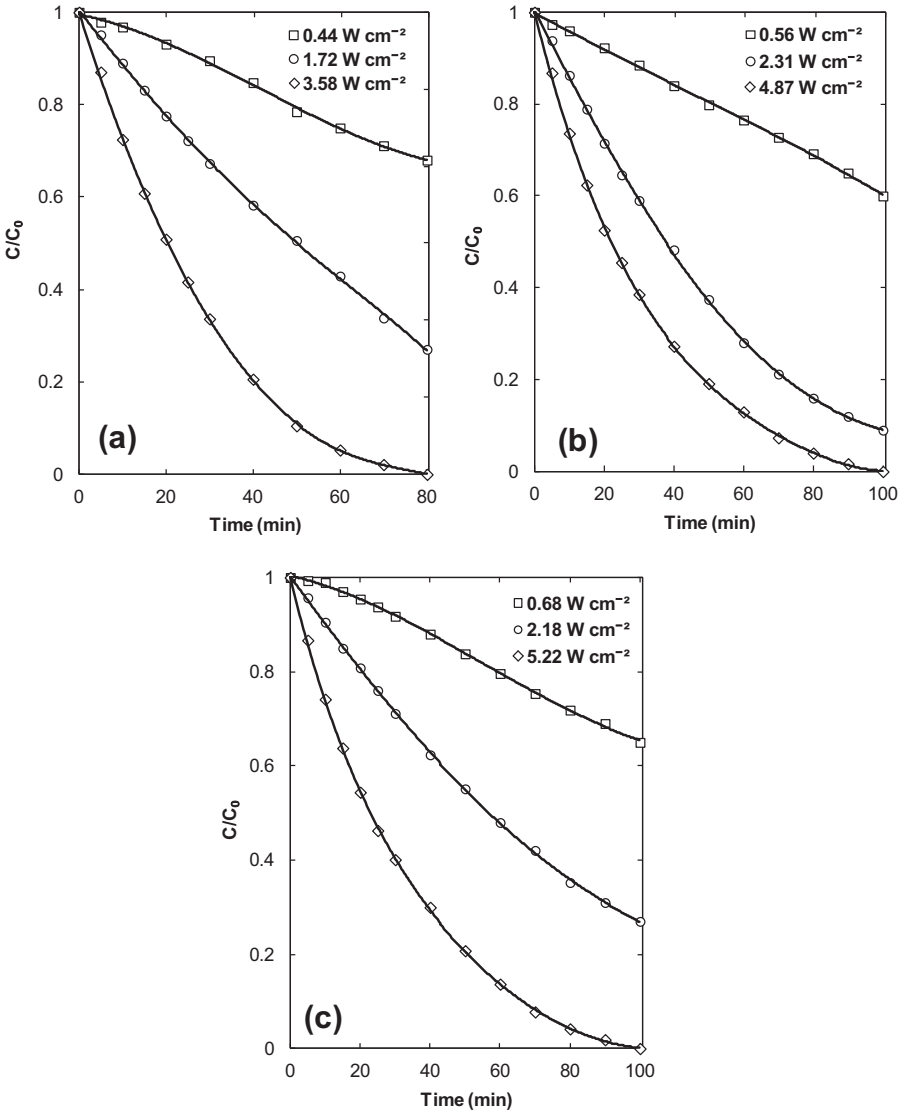

Fig. 4. Kinetics of the sonochemical degradation of NBB at (a) 585 kHz, (B) 860 kHz and (c) 1140 kHz and over a wide range of acoustic intensity (conditions: volume: 300 mL, initial NBB concentration: 30 mg L^{-1}, temperature: 25 °C, natural pH).

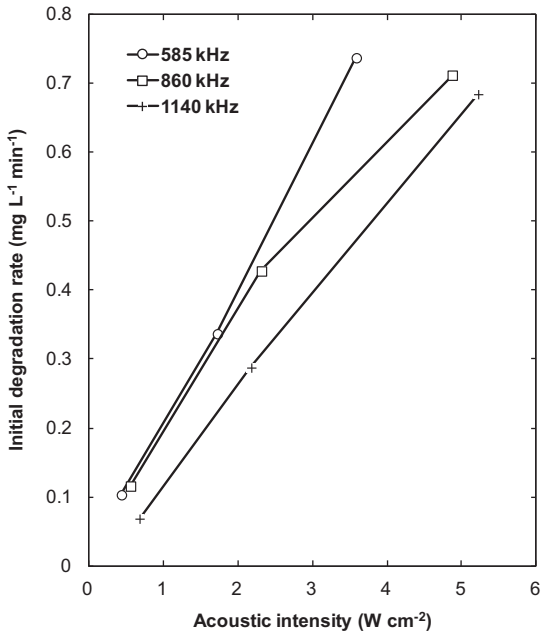

Fig. 5. Initial degradation rate of NBB as function of acoustic intensity at various frequencies (conditions: volume: 300 mL, initial NBB concentration: 5 mg L^{-1}, temperature: 25 °C, natural pH, acoustic intensity: 0.44–5.22 W cm^{-2}).

closes around a mean ambient radius [53]. The mean ambient bubble radius decreases considerably as ultrasonic frequency increases [53,54]. The ambient bubble radius (R_0) in the present numerical simulations has been assumed as the mean ambient bubble radius and the selected values, according to the experimental results [53,55], are 3.5 μm at 585 kHz, 2.7 μm at 860 kHz and 1.4 μm at 1140 kHz.

In Fig. 6(a)–(d), the results of the numerical simulations have been shown at an ultrasonic frequency of 585 kHz and different acoustic intensities. In Fig. 6(a), the R/R_0 ratios have been shown as function of time for the whole lifetime of the bubble. It was seen that the bubble initially expands to reach a maximum size and then quickly collapses to a minimum size and expands again. The bubble dynamics is strongly affected by the acoustic intensity. From the first view, it was remarked that the maximum bubble radius (R_{max}), the bubble lifetime and the bubble collapse time increase as the acoustic intensity increases. In Fig. 6(b), the bubble wall speeds have been shown as function of time for the same conditions as in Fig. 6(a). It was observed that the bubble wall velocity is not important during the expansion phase of the bubble and at the first stage of the collapse, but it increases suddenly during the final stage of the collapse up to 24, 97 and 171 m s^{-1} at respectively 0.44, 1.72 and 3.58 W cm^{-2}. These high speeds of implosion yield stronger collapses, which generate extremely higher conditions inside the bubbles. Indeed, the bubble internal pressure may increase up to 32, 400 and 1138 atm at the end of the bubble collapse at 0.44, 1.72 and 3.58 W cm^{-2}, respectively (Fig. 6(c)). Correspondingly, the temperature inside a bubble attained 1147, 2950 and 4190 K at the end of the bubble collapse at respectively 0.44, 1.72 and 3.58 W cm^{-2} (Fig. 6(d)). Such extreme conditions provide a unique environment where high-energy chemical reactions occur.

In Fig. 7, an enlargement view of the chemical reactions occurring in the bubble at the final stage of the bubble collapse as well as the bubble temperature has been shown as function of time at an ultrasonic frequency of 585 kHz and an acoustic intensity of 3.58 W cm^{-2}. For a liquid saturated with air, the main initial bubble content is air and water vapor. When the temperature and pressure in the bubble increased drastically, chemical reaction occurred in time scale of several nanoseconds (~20 ns) and many chemical products such as ·OH, O, H·, HO_2· H_2O_2, O_3, NO_2, NO_3, HNO_2 and HNO_3 are created from the dissociation of water vapor and gases molecules and their associate reactions. Among all the oxidants created in the bubble, only ·OH radical and O atom are formed at appreciable amount. They constitute more than 95% of the total amount of the oxidants formed in the bubble (~60% ·OH and ~35% O). In particular, ·OH radical has been specifically identified in sonicated aqueous solution via electron spin resonance [56] and is considered the primary oxidizing species during aqueous sonolysis because of its high potential of oxidation than the other oxidants formed in the bubble. Therefore, the numerical results revealed that the attack by ·OH radicals is the main pathway of NBB degradation in the aqueous phase. From Fig. 7, it was also seen that the amount of each chemical oxidant attained their upper limit near the end of the bubble collapse (at R_{min}), followed by almost constant production after the end of the bubble collapse as the bubble temperature decreases suddenly. In the following, the production rate of each oxidant is defined as the amount of this species after it become constant after the end of the first bubble collapse (the maximum yield) multiplied by the ultrasonic frequency [38]. In addition, as ·OH radical is the main species involved in the degradation of NBB, only the production rate of this species under the experimental conditions was examined.

In Fig. 8, the production rate of ·OH radical from a single oscillating bubble is shown as a function of acoustic intensity at various frequencies (conditions of the experimental results). The vertical axis in this figure is in logarithmic scale. The production rate of ·OH radical increased substantially with increasing acoustic intensity and decreased with increasing ultrasonic frequency, showing a good concordance with the experimental NBB degradation rate (Fig. 5). Thus, just by considering the chemical single-bubble yield, the observed trend in Fig. 5 can be qualitatively explained. However, a quantitative comparison between the single bubble yield and the overall degradation rate as a function of acoustic intensity cannot be established simply by considering numerical calculations based on single bubble yield.

The trend obtained in Fig. 8 results from the interaction between several dynamic parameters, principally, the amount of water vapor trapped at the collapse, the maximum temperature and pressure attained at the collapse and the bubble collapse time which control the extent of radicals production in the bubble. The effects of frequency and acoustic intensity on the dynamic parameters as well as the radical generation in the bubble are well detailed in our previous works [45,57].

4.2.2. Bubble number-dependence of frequency and acoustic intensity

The population, i.e., number and size, of cavitation bubbles also depends on the frequency of irradiation and the acoustic intensity. Experimental studies concerning the bubble number in an acoustic field is scarce. However, it is acknowledged that higher irradiation frequencies produce a greater number of cavitation bubbles [27,58,59]. It has been predicted [31] that the number of active cavitation bubbles increases with an increase in the ultrasound frequency in the range of 585–1140 kHz, which indicates that cavitation activity and hence the degradation efficiency can be expected to increase with an increase in frequency. However, the observed degradation results (Fig. 5) show the opposite trend. What this indicates is that of the two factors, the singe-bubble event and the number of active bubbles, the singe-bubble event must be the dominant factor that governs the overall sonochemical degradation rate of the dye in the range of 585–1140 kHz of frequency.

Several studies [25–27,30,60] showed the existence of an optimum frequency in the range of 200–500 kHz for sonochemistry. In this work, the range of the investigated frequency is 585–1140 kHz. The chemical efficiency from single bubble

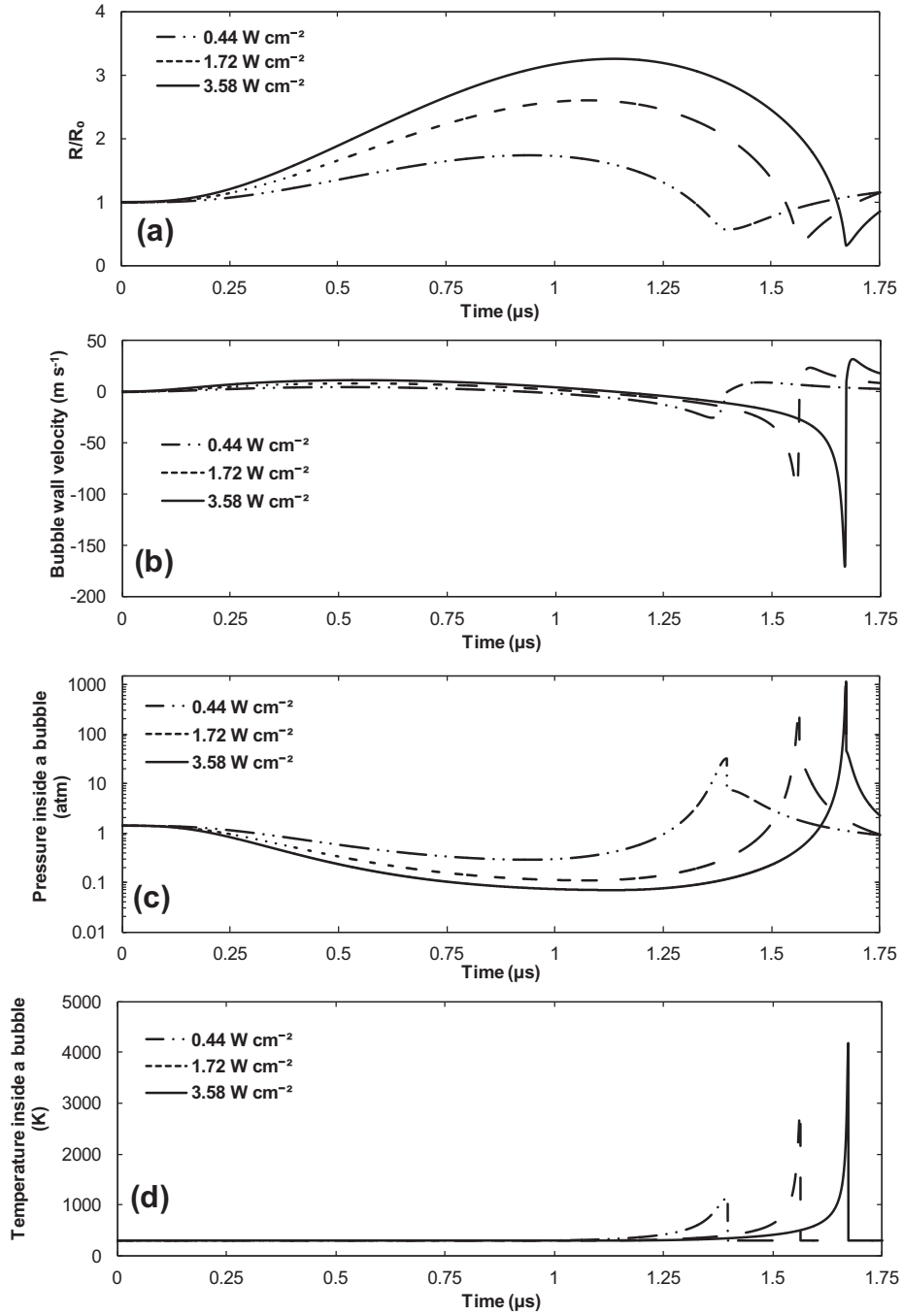

Fig. 6. The calculated results of the bubble radius (a), the bubble wall velocity (b), the pressure inside a bubble (c) and the temperature inside a bubble (d) as function of time for the whole lifetime of the bubble at 585 kHz and various acoustic intensities (conditions: ambient bubble radius: 3.5 μm, liquid temperature: 25, static pressure: 1 atm). The vertical axis in (c) is in logarithmic scale.

monotonically decreased with the frequency increase in this range (Fig. 8), and it, qualitatively, agrees with the results in the studies mentioned above. However, previous numerical computations [61] have also demonstrated the existence of an optimum frequency (~500 kHz) for the production of ·OH radical in single bubble when the liquid is saturated with argon. For all other saturation gases (air, O_2 and N_2), the simulations results indicated that the single chemical bubble yield decreased sharply with frequency increase in the range of 213–1100 kHz [61]. At this level, it should be mentioned that the overall sonochemical efficiency cannot be associated only to the single bubble event but also to the number of active bubbles which is another important parameters in aqueous sonochemistry (multibubble system). It was proven experimentally that the number of active bubbles increases with frequency increase (the zones of cavitation field [59] and sonochemiluminescence [62] in water were much extended at high frequency compared to those observed at lower frequency). Therefore, by considering or no of the existence of an optimum frequency for single bubble sonochemistry, the chance of obtaining an optimum frequency between 200 and 1000 kHz for aqueous sonochemistry is possible as it can be resulted from the competition between two factors: the sonochemical activity in individual bubble, which decreased with increasing frequency (excepting the case of argon saturation) and the number of active bubbles, which increases with

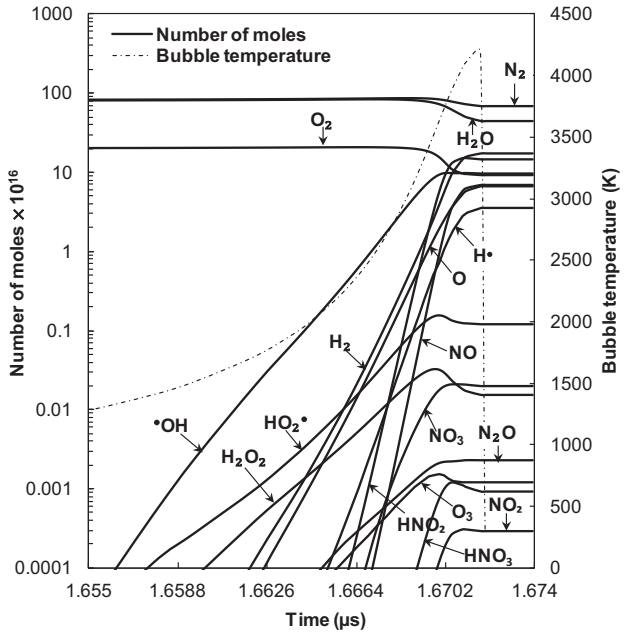

Fig. 7. A typical case for the evolution of the reaction system inside a bubble as function of time at around the end of the bubble collapse (conditions: ultrasonic frequency: 585 kHz, acoustic intensity: 3.58 W cm^{-2}, static pressure: 1 atm, liquid temperature: 25 °C). The principal vertical axis is in logarithmic scale. The horizontal axis is only for about 0.02 μs. The numerical simulation of chemical reactions was conducted for a bubble initially composed of air and water vapor.

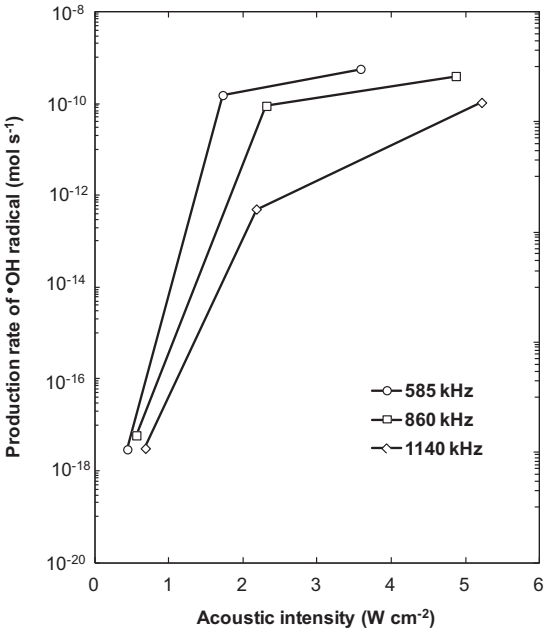

Fig. 8. The calculated production rate of ·OH radical inside a single bubble as function of acoustic intensity at various frequencies (conditions: ambient bubble radius: 5 μm at 585 kHz, 2.7 μm at 860 kHz and 1.4 μm at 1140 kHz, bulk liquid temperature: 20 °C, static pressure: 1 atm). The vertical axis is in logarithmic scale. The production rate of ·OH is defined as the amount of this species after it become constant after the end of the first bubble collapse multiplied by the ultrasonic frequency [38].

increasing frequency. However, in the absence of exact information about the bubble number, any theoretical decision about the existing of an optimum frequency for sonochemistry is not possible to make.

The number of active cavitation bubbles may also increases with an increase in acoustic intensity between the Black and the attenuated thresholds [58,63]. Whereas the effect of acoustic intensity, shown in Fig. 5, has been interpreted on the basis of the single bubble yield, an increase in the number of bubbles may also explain the observed trends.

Consequently, it can be concluded that:

- The observed effect of acoustic intensity on the sonochemical degradation rate of NBB is the direct result of the increase of both the single bubble yield and the number of active bubbles with increasing acoustic intensity in the interval 0.44–5.22 W cm^{-2}.
- The observed effect of frequency in the range 585–1140 kHz on the degradation rate of the dye is predominately attributed to its significant impact on single bubble yield, which was found lesser efficient at higher frequencies (Fig. 8).

5. Conclusion

In this study, the sonochemical degradation of NBB, an acidic dye largely used in textile industry, in water have been investigated experimentally and theoretically at various frequencies and different acoustic intensities. The observed experimental results have been discussed with respect to single bubble sonochemistry and the number of active bubbles. This approach of interpretation is rarely used as the most numerical studies reported in the literature used only the output parameters of a bubble dynamics model (the maximum bubble temperature and pressure) to interpret the results. The internal bubble-chemistry is not affected only by the bubble temperature and pressure but also to other important parameters such as the bubble composition in water vapor and gases, the time of the bubble collapse and the bubble volume. All these parameters were taken into account in our model to simulate the internal bubble chemistry and, thus, the numerical calculations will generate more realistic interpretations. After estimating the production rate of ·OH inside a single oscillating bubble under the operating conditions of the experiments, it has been concluded that the overall production rate of NBB is controlled by the single bubble event and the number of active bubbles. The enhancing effect of acoustic intensity toward the sonolytic degradation rate was attributed to the rise of both the individual chemical bubble yield and the number of active bubbles with increasing acoustic intensity. The reducing effect of frequency was attributed to the sharp decrease in the chemical bubble yield with increasing frequency.

Acknowledgements

The financial support by the Ministry of Higher Education and Scientific Research of Algeria (project No. J0101120120098) is greatly acknowledged.

References

[1] H. Ghodbane, O. Hamdaoui, Intensification of sonochemical decolorization of anthraquinonic dye Acid Blue 25 using carbon tetrachloride, Ultrason. Sonochem. 16 (2009) 455–461.
[2] I.G. Laing, The impact of effluent regulations on the dyeing industry, Rev. Prog. Color. 21 (1991) 56–71.
[3] I. Gültekin, G. Tezcanli-Güyer, N.H. Ince, Sonochemical decay of C.I. Acid Orange 8: effects of CCl4 and t-butyl alcohol, Ultrason. Sonochem. 16 (2009) 577–581.
[4] G.N.P. Kumar, K.B. Sumangala, Decolorization of azo dye Red 3BN by bacteria, Int. Res. J. Biol. Sci. 1 (2012) 46–52.
[5] A. Pandey, P. Singh, L. Iyengar, Bacterial decolorization and degradation of azo dyes, Int. Biodeterior. Biodegrad. 59 (2007) 73–84.

[6] A.L. Ahmad, S.W. Puasa, Reactive dyes decolourization from an aqueous solution by combined coagulation/micellar-enhanced ultrafiltration process, Chem. Eng. J. 132 (2007) 257–265.
[7] B. Shi, G. Li, D. Wang, C. Feng, H. Tang, Removal of direct dyes by coagulation: the performance of preformed polymeric aluminum species, J. Hazard. Mater. 143 (2007) 567–574.
[8] J.H. Mo, Y.H. Lee, J. Kim, J.Y. Jeong, J. Jegal, Treatment of dye aqueous solutions using nanofiltration polyamide composite membranes for the dye wastewater reuse, Dyes Pigm. 76 (2008) 429–434.
[9] E.N. El Qada, S.J. Allen, G.M. Walker, Adsorption of basic dyes from aqueous solution onto activated carbons, Chem. Eng. J. 135 (2008) 174–184.
[10] B.H. Hameed, A.A. Ahmad, N. Aziz, Isotherms, kinetics and thermodynamics of acid dye adsorption on activated palm ash, Chem. Eng. J. 133 (2007) 195–203.
[11] S. Boutemedjet, O. Hamdaoui, Sorption of Malachite green by eucalyptus bark as a non-conventional low-cost biosorbent, Desalin. Water Treat. 8 (2009) 201–210.
[12] N. Tripathy, R. Ahmad, J.E. Song, H.A. Ko, Y.-B. Hahn, G. Khang, Photocatalytic degradation of methyl orange dye by ZnO nanoneedle under UV irradiation, Mater. Lett. 136 (2014) 171–174.
[13] K. Dutta, S. Bhattacharjee, B. Chaudhuri, S. Mukhopadhyay, Chemical oxidation of C. I. Reactive Red 2 using Fenton-like reactions, J. Environ. Monit. 4 (2002) 754–760.
[14] A. Aleboyeh, M.B. Kasiri, M.E. Olya, H. Aleboyeh, Prediction of azo dye decolorization by UV/H_2O_2 using artificial neural networks, Dyes Pigm. 77 (2008). 288e294.
[15] H.J. Hsing, P.C. Chiang, E.E. Change, M.Y. Chen, The decolorization and mineralization of Acid Orange 6 azo dye in aqueous solution by advanced oxidation processes: a comparative study, J. Hazard. Mater. 141 (2007) 8–16.
[16] Y.G. Adewuyi, Sonochemistry: environmental science and engineering applications, Ind. Eng. Chem. Res. 40 (2001) 4681–4715.
[17] M.R. Hoffmann, I. Hua, R. Höchemer, Application of ultrasonic irradiation for the degradation of chemical contaminants in water, Ultrason. Sonochem. 3 (1996) S163–S172.
[18] L.H. Thompson, L.K. Doraiswamy, Sonochemistry: science and engineering, Ind. Eng. Chem. Res. 38 (1999) 1215–1249.
[19] K.S. Suslick, Y. Didenko, M.M. Fang, T. Hyeon, K.J. Kolbeck, W.B. McNamara, M.M. Mdleleni, M.M. Wong, Acoustic cavitation and its chemical consequences, Philos. Trans. R. Soc. A: Math. Phys. Eng. Sci. 357 (1999) 335–353.
[20] P. Riesz, D. Berdahl, C.L. Christman, Free radical generation by ultrasound in aqueous and nonaqueous solutions, Environ. Health Perspect. 64 (1985) 233–252.
[21] C. Pétrier, Y. Jiang, M.-F. Lamy, Ultrasound and environment: sonochemical destruction of chloroaromatic derivatives, Environ. Sci. Technol. 32 (1998) 1316–1318.
[22] M. Capocelli, E. Joyce, A. Lancia, T.J. Mason, D. Musmarra, M. Prisciandaro, Sonochemical degradation of estradiols: incidence of ultrasonic frequency, Chem. Eng. J. 210 (2012) 9–17.
[23] M. Dukkanci, M. Vinatoru, T.J. Maison, Sonochemical treatment of orange II using ultrasound at range of frequencies and powers, J. Adv. Oxid. Technol. 15 (2012) 277–283.
[24] F. Méndez-Arriaga, R.A. Torres, C. Pétrier, S. Esplugas, J. Gimenez, C. Pulgarin, Ultrasonic treatment of water contaminated with ibuprofen, Water Res. 42 (2008) 4243–4248.
[25] R.A. Torres, C. Pétrier, E. Combet, M. Carrier, C. Pulgarin, Ultrasonic cavitation applied to the treatment of bisphenol A. Effect of sonochemical parameters and analysis of BPA by-products, Ultrason. Sonochem. 15 (2008) 605–611.
[26] Y. Jiang, C. Petrier, T.D. Waite, Sonolysis of 4-chlorophenol in aqueous solution: effects of substrate concentration, aqueous temperature and ultrasonic frequency, Ultrason. Sonochem. 13 (2006) 415–422.
[27] M.A. Beckett, I. Hua, Impact of ultrasonic frequency on aqueous sonoluminescence and sonochemistry, J. Phys. Chem. A 105 (2001) 3796–3802.
[28] S. Onder, M. Celebi, M. Altikatoglu, A. Hatipoglu, H. Kuzu, Decolorization of naphthol blue black using the horseradish peroxidase, Appl. Biochem. Biotechnol. 163 (2011) 433–443.
[29] T.J. Mason, J.P. Lorimer, D.M. Bates, Quantifying sonochemistry: casting some light on a 'black art', Ultrasonics 30 (1992) 40–42.
[30] S. Koda, T. Kimura, T. Kondo, H. Mitome, A standard method to calibrate sonochemical efficiency of an individual reaction system, Ultrason. Sonochem. 10 (2003) 149–156.
[31] S. Merouani, O. Hamdaoui, Y. Rezgui, M. Guemini, A method for predicting the number of active bubbles in sonochemical reactors, Ultrason. Sonochem. 22 (2015) 51–58.
[32] S. Merouani, O. Hamdaoui, Y. Rezgui, M. Guemini, Energy analysis during acoustic bubble oscillations: relationship between bubble energy and sonochemical parameters, Ultrasonics 54 (2014) 227–232.
[33] L.A. Crum, The polytrophic exponent of gas contained within air bubbles pulsating in a liquid, J. Acoust. Soc. Am. 73 (1983) 116–120.
[34] J.B. Keller, I.I. Kolodner, Damping of underwater explosion bubble oscillations, J. Appl. Phys. 27 (1956) 1152–1161.
[35] J.B. Keller, M.J. Miksis, Bubble oscillations of large amplitude, J. Acoust. Soc. Am. 68 (1980) 628–633.
[36] K. Yasui, Fundamental of acoustic cavitation and sonochemistry, in: Pankaj, M. Ashokkumar (Eds.), Theoretical and Experimental Sonochemistry Involving Inorganic Sonochemistry, Springer, London, 2001, pp. 1–29. Chapter 1.
[37] K. Yasui, T. Tuziuti, M. Sivakumar, Y. Iida, Theoretical study of single bubble sonochemistry, J. Chem. Phys. 120 (2005) 224706-1–224706-12.
[38] K. Yasui, T. Tuziuti, J. Lee, T. Kozuka, A. Towada, The range of ambient radius for an active bubble in sonoluminescence and sonochemical reactions, J. Chem. Phys. 128 (2008) 184705.
[39] A.J. Colussi, L.K. Weavers, M.R. Hoffmann, Chemical bubble dynamics and quantitative sonochemistry, J. Phys. Chem. A 102 (1998) 6927–6934.
[40] N.P. Vichare, P. Senthilkumar, V.S. Moholkar, P.R. Gogate, A.B. Pandit, Energy analysis in acoustic cavitation, Ind. Eng. Chem. Res. 39 (2000) 1480–1486.
[41] K. Yasui, Effect of non-equilibrium evaporation and condensation on bubble dynamics near the sonoluminescence threshold, Ultrasonics 36 (1998) 575–580.
[42] B.D. Storey, A.J. Szeri, Water vapor, sonoluminescence and sonochemistry, Proc. R. Soc. Lond. A 456 (2000) 1685–1709.
[43] V. Kamath, A. Prosperetti, F.N. Egolfopoulos, A theoretical study of sonoluminescence, J. Acoust. Soc. Am. 94 (1993) 248–260.
[44] S. Fujikawa, T. Akamatsu, Effects of the non-equilibrium condensation of vapour on the pressure wave produced by the collapse of a bubble in a liquid, J. Fluid Mech. 97 (1980) 481–512.
[45] S. Merouani, O. Hamdaoui, Y. Rezgui, M. Guemini, Sensitivity of free radicals production in acoustically driven bubble to the ultrasonic frequency and nature of dissolved gases, Ultrason. Sonochem. 22 (2015) 41–50.
[46] M.O. Conaire, H.J. Curran, J.M. Simmie, W.J. Pitz, C.K. Westbrook, A comprehensive modeling study of hydrogen oxidation, Int. J. Chem. Kinet. 36 (2004) 603–622.
[47] M.A. Mueller, T.J. Kim, R.A. Yetter, F.L. Dryer, Flow reactor studies and kinetic modeling of the H_2/O_2 reaction, Int. J. Chem. Kinet. 31 (1999) 113–125.
[48] NIST Chemical Kinetics Database (2011), http://kinetics.nist.gov/kinetics/index.jsp.
[49] A. Henglein, M. Gutierrez, Chemical effects of continuous and pulsed ultrasound: a comparative study of polymer degradation and iodide oxidation, J. Phys. Chem. 92 (1988) 5169–5172.
[50] O. Moumeni, O. Hamdaoui, C. Pétrier, Sonochemical degradation of malachite green in water, Chem. Eng. Process. 62 (2013) 47–53.
[51] Data sheet of Naphthol blue black in *PubChem*, http://pubchem.ncbi.nlm.nih.gov/summary/sum mary.cgi?sid=87560295.
[52] S. Dalhatou, C. Pétrier, S. Laminsi, S. Baup, Sonochemical removal of naphthol blue black azo dye: influence of parameters and effect of mineral ions, Int. J. Environ. Sci. Technol. 12 (2015) 35–44.
[53] A. Brotchie, F. Grieser, M. Ashokkumar, Effect of power and frequency on bubble-size distributions in acoustic cavitation, Phys. Rev. Lett. 102 (2009) 084302-1–084302-4.
[54] S. Labouret, J. Frohly, Distribution en tailles des bulles d'un champ de cavitation ultrasonore, 10ème Congrès Français d'Acoustique, Lyon, 2010, http://hal.archives-ouvertes.fr/docs/00/55/11/51/PDF/000441.pdf.
[55] W.-S. Chen, T.J. Matula, L.A. Crum, The disappearance of ultrasound contrast bubbles: observations of bubble dissolution and cavitation nucleation, Ultrasound Med. Biol. 28 (2002) 793–803.
[56] K. Makino, M.M. Mossoba, P. Riesz, Chemical effects of ultrasound on aqueous solutions. Formation of hydroxyl radicals and hydrogen atoms, J. Phys. Chem. 87 (1983) 1369–1377.
[57] S. Merouani, O. Hamdaoui, Y. Rezgui, M. Guemini, Computer simulation of chemical reactions occurring in collapsing acoustical bubble: dependence of free radicals production on operational conditions, Res. Chem. Intermed. 41 (2015) 881–897.
[58] P. Kanthale, F. Ashokkumar, F. Grieser, Sonoluminescence, sonochemistry (H_2O_2 yield) and bubble dynamics: frequency and power effects, Ultrason. Sonochem. 15 (2008) 143–150.
[59] J. Lee, M. Ashokkumar, K. Yasui, T. Tuziuti, T. Kozuka, A. Towata, Y. Iida, Development and optimization of acoustic bubble structures at high frequencies, Ultrason. Sonochem. 18 (2011) 92–98.
[60] T. Kondo, E. Kano, Effect of free radicals induced by ultrasonic cavitation on cell killing, Int. J. Radiat. Biol. 54 (1988) 475–486.
[61] S. Merouani, O. Hamdaoui, Y. Rezgui, M. Guemini, New interpretation of the effects of argon-saturating gas toward sonochemical reactions, Ultrason. Sonochem. 23 (2015) 37–45.
[62] C. Pétrier, M.F. Lamy, A. Francony, A. Benahcene, B. David, Sonochemical degradation of phenol in dilute aqueous solutions: comparison of the reaction rates at 20 and 487 kHz, J. Phys. Chem. 98 (1994) 10514–10520.
[63] D. Sunartio, M. Ashokkumar, F. Grieser, Study of the coalescence of acoustic bubbles as a function of frequency, power, and water-soluble additives, J. Am. Chem. Soc. 129 (2007) 6031–6036.